The Interaction of Numerically Simulated Supercells Initiated along Lines

HOWARD B. BLUESTEIN

School of Meteorology, University of Oklahoma, Norman, Oklahoma

MORRIS L. WEISMAN

National Center for Atmospheric Research, Boulder, Colorado*

(Manuscript received 20 August 1999, in final form 19 January 2000)

ABSTRACT

Supercells in the southern plains are often localized, forming as cells along a convective line, even though the environment may support supercell formation over a much broader, mesoscale region. A set of numerical experiments is devised in which it is demonstrated that the evolution of supercells in a homogeneous environment depends upon the orientation of the vertical-shear profile with respect to the orientation of the line along which convection is initiated (the ''line of forcing''). This work is motivated by the observations that the nature and consequences of the interaction of neighboring cells depend upon differential cell motion, which in turn is a function of the characteristics and orientation of the vertical-shear profile and its impact on the behavior of outflow boundaries.

Results for various orientations of the vertical-shear vector with respect to the line along which cells are initiated are described and interpreted physically. It is found that in idealized numerical simulations, shear oblique to (45° from) the line of forcing is most apt to support neighboring cyclonic supercells within the line, but also supports an anticyclonic supercell at the downshear end of the line; shear normal to the line of forcing is favorable for the maintenance of a squall line with isolated supercells at either end; shear parallel to the line of forcing is favorable for isolated supercells only on the downshear side of the line. The effects of low-level clockwise curvature in the hodograph vary from case to case, depending upon the orientation of the leading edges of the system cold pool with respect to the low-level shear. Differences in low-level static stability and the dryness of air aloft affect storm behavior less than differences in the orientation of the vertical shear. The process of storm collision is examined in detail.

1. Introduction

A supercell is a long-lived convective storm whose behavior is dictated by a rotating updraft that is dynamically generated by the interactions between the buoyant updraft and strong environmental vertical wind shear. It is meteorologically important because of its ability to spawn severe weather phenomena such as tornadoes and large hail. Supercells tend to move differently from the pressure-weighted mean wind mainly as a result of rotationally induced perturbations in the dynamic part of the pressure field: cells have a component of propagation normal to the shear, and these can move either to the right or left of the mean wind. When the hodograph is curved in a clockwise (counterclockwise) manner with height, the cyclonic right movers (anticyclonic left movers) are favored. The motion of gust fronts generated by evaporating precipitation also influences storm movement and can trigger additional cells.

It is well known based upon observations (e.g., Marwitz 1972a–c; Bluestein and Parker 1993) and numerical simulation experiments (Weisman and Klemp 1982, 1984) that supercells form in environments having values of moderate to high vertical wind shear, along with some convective available potential energy (CAPE). In particular, supercell processes become significant when the vertical shear exhibits at least 20–25 m s^{-1} of wind variation over the lowest 4–6 km above ground level (AGL). These criteria, however, are necessary but not sufficient conditions for supercell formation. Such conditions often exist over a relatively broad, mesoscale region, but generally only a small percentage of the cells that develop within such a region become supercellular. There are many possible reasons for this behavior, including unobserved mesoscale variations in environmental conditions, detrimental interactions between neighboring cells, etc.

* The National Center for Atmospheric Research is sponsored by the National Science Foundation.

Corresponding author address: Dr. Howard B. Bluestein, School of Meteorology, University of Oklahoma, 100 E. Boyd, Rm. 1310, Norman, OK 73019.
E-mail: hblue@ou.edu

The character of the convective triggering may also be important. Supercells are inherently three-dimensional; isolated cells are generally more likely to develop supercellular characteristics than those that develop within a system such as a squall line. However, more often than not, cells are triggered along a line segment, and thus the possibility of interactions with neighboring cells is a common occurrence. For instance, Bluestein and Parker (1993) and Bluestein and MacGorman (1998) found that supercells along the dryline in the southern plains often begin as line segments of isolated cells, which apparently interact as they evolve. Bluestein and Jain (1985) found that severe squall lines initiated along cold fronts frequently begin as a ''broken line'' of cells. Other detailed case studies of supercell formation and evolution (e.g., Burgess and Curran 1985; Bluestein et al. 1988; Bluestein and Woodall 1990; Bluestein and Hutchinson 1996) show how adjacent cells initiated along a line segment can interact with each other to favor the evolution of one or more of the cells into a supercell (Fig. 1). For convective storms that do form along quasi-linear surface boundaries, why is it that some boundaries or sections of boundaries are more conducive for supercell formation than others?

Some guidance as to how supercell storms are apt to interact along a line can be obtained from previous numerical and theoretical studies. Such studies have suggested a relationship between storm structure and both the geometry of the convective storms and of the vertical wind shear vector in the environment. For instance, Lilly (1979) considered how neighboring isolated storms arranged in a line may constructively or destructively interfere with each other as a result of differential propagation. Wilhelmson and Klemp (1983) subsequently studied numerically simulated storms triggered along an infinitely long line; they used a periodic domain in which storms were triggered every 40 km. Although they considered interactions with neighboring storms, they considered only a limited number of cases, and did not consider what happens to cells at the ends of a line. Rotunno et al. (1988) and Weisman et al. (1988) conducted numerical experiments with an infinitely long line thermal, upon which are superimposed small random perturbations, in an environment having deep, strong shear at various angles with respect to the line thermal. They found that for shear oriented 45° to the line, a line of discrete supercells evolves because each supercell can persist without interference from its neighbors.

We can summarize these previous studies by considering a line segment of a stationary boundary along which convective storms are initiated simultaneously at several locations. Suppose, for simplicity, that the environmental hodograph has strong, unidirectional shear, such that mirror image splitting supercells would result. Also, let us assume that no new cells are triggered along the storm-generated surface outflow boundaries. If the boundary along which storms are initiated is oriented in the north–south direction in a westerly sheared environment, then it is expected that a series of left-moving and right-moving storms will be generated; the right-moving storms will collide with the left-moving storms to their south; only the southernmost right-moving and northernmost left-moving storms will likely not interact with their neighbors (Fig. 2a). If, however, the shear is oriented at a 45° angle to the boundary, then, with the exception of the northernmost storm, the left-moving members will move across the outflow boundary generated by their right-moving neighbor to the north, and weaken, while the right-moving members will move away from the boundary and may not collide with their neighbors (Fig. 2b). Finally, if the shear is oriented parallel to the boundary, then the left movers will move behind the boundary, while the right movers will slowly move ahead of the boundary (Fig. 2c). However, since there is also a component of storm motion parallel to the boundary, the right movers might catch up to the outflow boundaries generated by the adjacent right movers along the line, and weaken. Only the downshear-most storms would be able to evolve without interacting with their neighboring cells.

We therefore expect that neighboring storms may, in some circumstances, interfere destructively with each other (Lilly 1979). Storm motion depends upon the magnitude and orientation of the vertical shear, the strength and orientation of gust fronts, and the orientation of the boundary along which the storms were triggered. Thus, storm evolution in an environment that is homogeneous on either side of a boundary along which storms are triggered will depend upon the orientation of the vertical shear profile with respect to the orientation of the boundary and whether or not a storm is an interior cell or at one of the ends of the line.

To see how these storm interaction processes relate to nowcasting and forecasting problems, consider two common synoptic patterns in the central region of the United States. Suppose the vertical shear is westerly. First, consider the case in which a dryline intersects a stationary front in the southern plains (Fig. 3a). The dryline is usually oriented in the north–south direction, while the front is often oriented in the east–west direction. If the environmental shear is westerly, the vertical shear vector is oriented normal to the dryline, but along the cold front.

Now consider the case in which a cyclone is located in the northern plains, and a cold front curves southward and southwestward into the southern plains (Fig. 3b). If the environmental hodograph is the same everywhere, then the vertical shear is normal to the front in the northern plains, at a 45° angle to the front to the south, and along the front far to the south. Although we are oversimplifying the relationship between the hodograph and the front, the overall relationship is still valid; for example, if the atmosphere is in near-thermal-wind balance, then the vertical-shear vector at low levels behind the front will necessarily be oriented along the front.

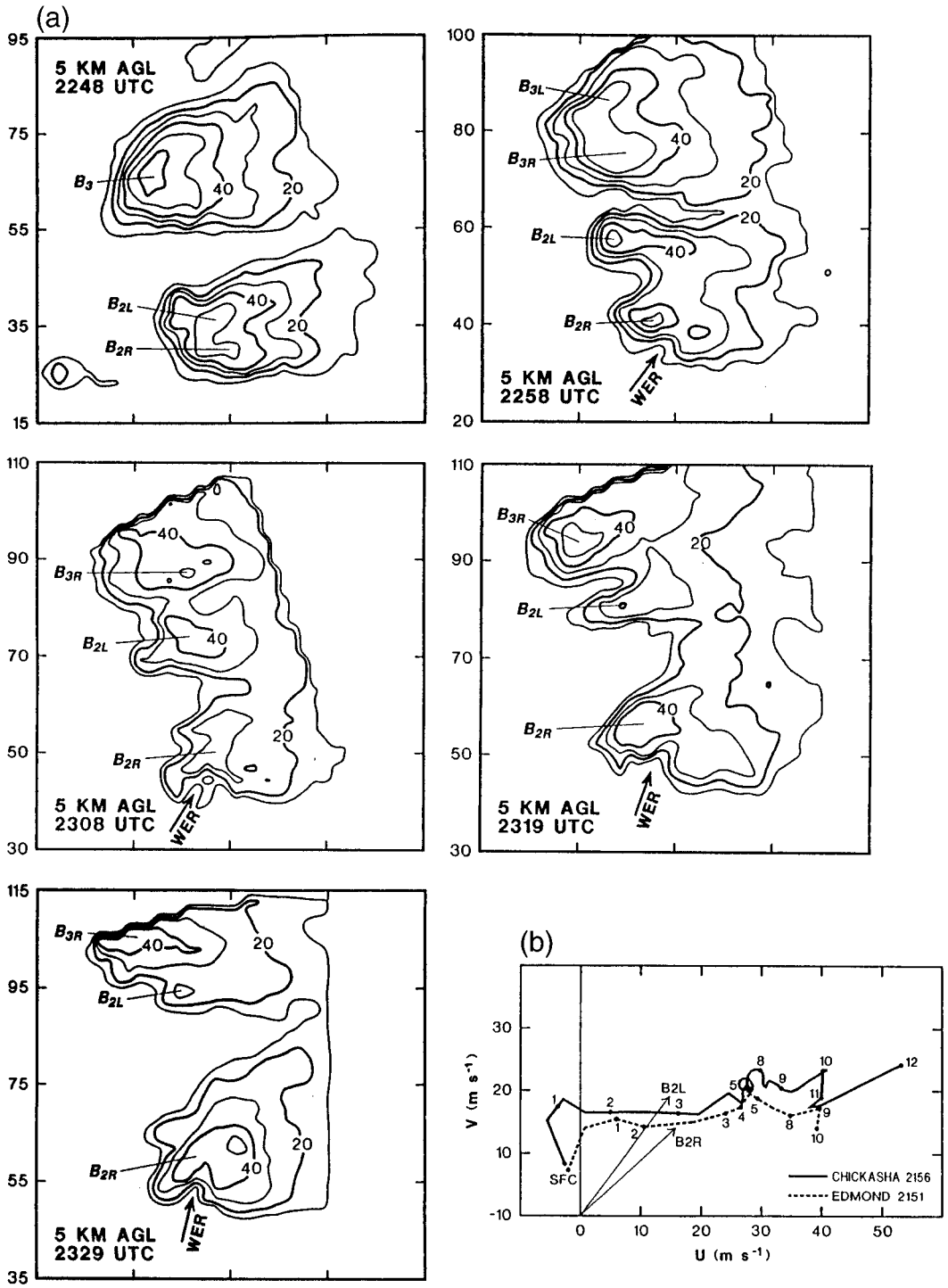

FIG. 1. (a) Radar reflectivity contours in dBZ at 10-dBZ intervals for the Norman Doppler radar at the National Severe Storms Laboratory on 26 Apr 1984, for the times indicated at 5 km AGL; outer reflectivity contour is 10 dBZ; no data are analyzed beyond 115 km from the radar. The distance (km) north of the radar is shown to the left of each panel; the tick marks in the east–west direction at the bottom of each panel represent increments of 20 km (from Fig. 17 of Bluestein and Woodall 1990). (b) Hodographs from soundings released near the storms when they were initiated (from Fig. 7 of Bluestein and Woodall 1990).

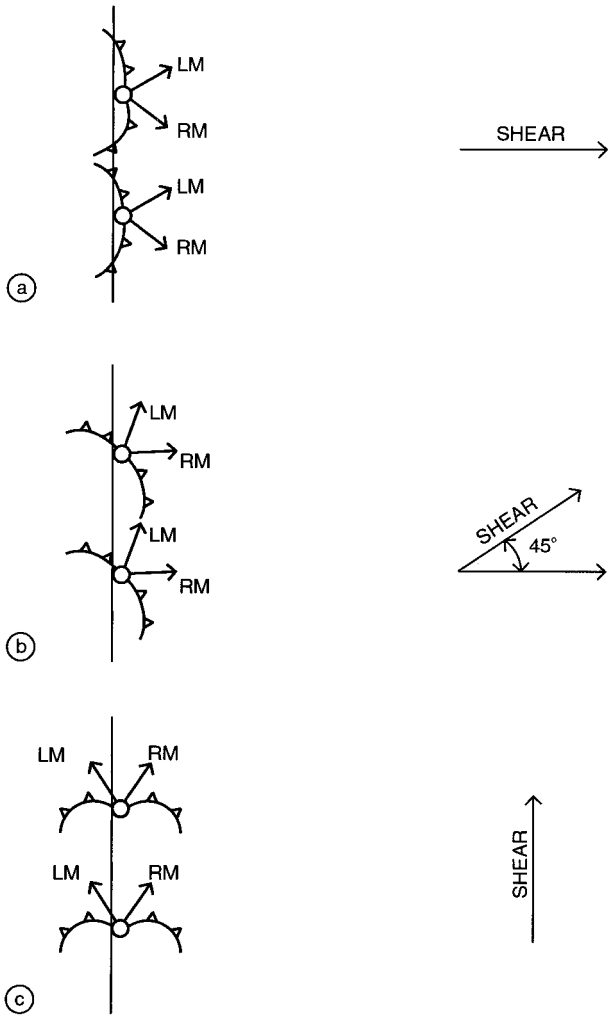

FIG. 2. Idealized illustration of the relationship between the orientation of the line of forcing (initial thermal bubbles indicated by circles along a vertical line) and the vertical-shear vector (at right). Outflow boundaries denoted by cold front symbol; RM and LM denote storm motion (vectors) of subsequent right- and left-moving cells.

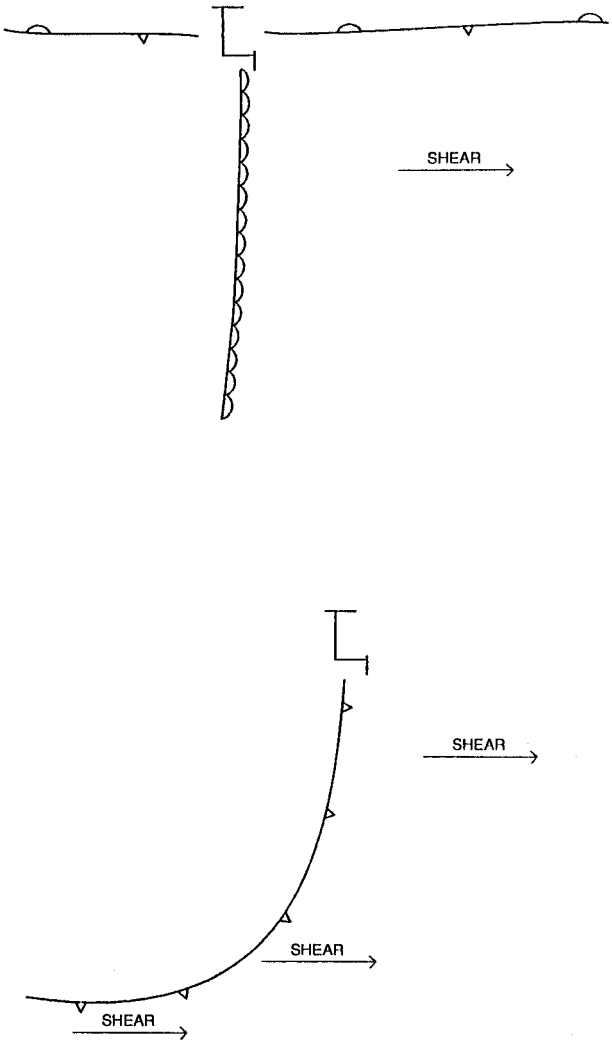

FIG. 3. Typical synoptic features at the surface in the plains region of the United States. (a) Dryline–front intersection, with low pressure area (cyclone). (b) Cold front and low pressure area (cyclone). Vectors represent vertical shear; L denotes low pressure area associated with the cyclone. Dryline in (a) is represented by a scalloped line.

However, we can assume that the depth of the front is only a small fraction of the depth of the troposphere and that most convection, even if initiated along the front, will move ahead of it.

The primary purpose of this paper is to demonstrate the storm interaction relationships along boundaries using controlled numerical simulation experiments. In nature, the environments on either side or on both sides of the boundary are not necessarily homogeneous, so that variations in boundary layer moisture and temperature can also play a role in determining where convection breaks out and how it evolves. Also, boundaries are not necessarily stationary. However, we ignore these complications in order to simplify the problem. A secondary purpose of this study is to examine storm interactions fairly early on in their history and to determine what happens when storms collide. We also will briefly examine the effects on storm evolution of low-level static stability, dryness aloft, and cross-boundary variations in dryness.

In section 2 we describe the methodology of our numerical experiments. The results of our simulations are detailed in section 3; a summary of our results and their implications are given in section 4.

2. Methodology of numerical experiment

We simulated convective storms using the Klemp–Wilhelmson cloud model (Klemp and Wilhelmson 1978) as has been done extensively, for example, by Weisman and Klemp (1982, 1984) for isolated convection and by Rotunno et al. (1988) and Weisman et al. (1988) for squall lines. Liquid-water cloud microphysics are sim-

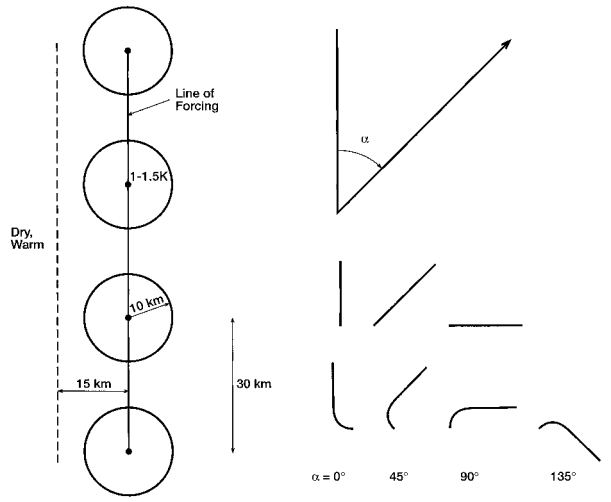

FIG. 4. Depiction of the numerical simulation experiments. Circles represent thermal bubbles. Hodographs for various orientations with respect to the line of forcing shown at the right; α is the angle measured in a clockwise manner between the line of forcing and the hodograph above 1.7 km AGL. Dashed line represents boundary between dry, warm air, and ambient air in some of the experiments.

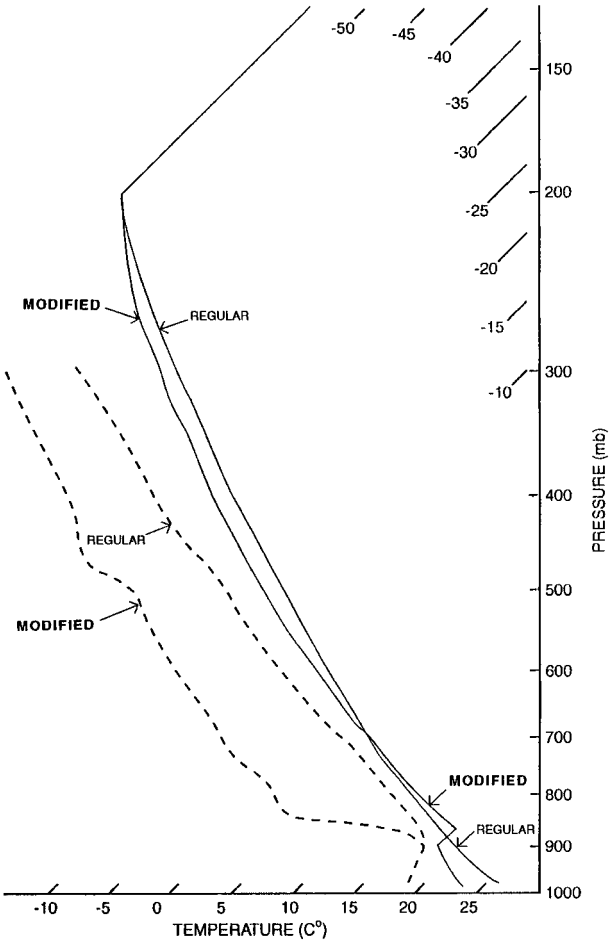

FIG. 5. The modified and unmodified (regular) Weisman and Klemp (1982) soundings used in the simulation experiments. Temperatures and dewpoints indicated in °C on the skewed scale; pressure is plotted in mb. Temperature plotted as solid lines; dewpoint plotted as dashed lines.

ulated using a Kessler parameterization scheme. The Coriolis force was not included in order to simplify the interpretation of our simulations, which are for only several hours duration or less.

To simulate the processes involved in neighboring cell interactions, we chose to initialize the model using four thermal bubbles, each neighboring pair spaced apart by 30 km (Fig. 4). With four bubbles, we can determine the difference in behavior between interacting neighboring cells and cells at the ends of the line, which may or may not interact with any neighbor at all, and we can keep the size of the domain of the model small enough to limit the required computation time. Unlike the simulations of lines of supercells done by Wilhelmson and Klemp (1983), Rotunno et al. (1988), and Weisman et al. (1988), in which there were no ends in the line, our simulations allow for the more realistic case of a finite line segment.

The spacing between thermal bubbles was chosen so that neighboring cells could interact after they had begun to develop supercell characteristics, which is usually at least 45 min or so after initiation. The geometry we use, furthermore, is similar to that of many storms in nature, early in the their life (e.g., Bluestein and Parker 1993; Bluestein et al. 1988; Bluestein and MacGorman 1998). In nature, cells are not necessarily triggered simultaneously, as in our experiments. However, we will not consider the triggering of cells by thermal bubbles at different times in order to keep the experiment simple.

Each thermal bubble had a horizontal radius of 10 km, a vertical radius of 1400 m, and was centered at 1400 m AGL. The maximum magnitude of the thermal bubble was 1–1.5 K; the magnitude of the temperature excess in the bubble decreased toward zero as the $\cos^2$ of the distance from the center. This thermal perturbation was near the minimum magnitude that would produce storm initiation within a reasonable time (i.e., 20–30 min) for all cases considered. Using the minimum perturbation is important to ensure that the long-term solutions are minimally affected by the nature of the initialization. For example, if the initial cell and its surface cold pool were unrealistically strong for the sounding, the character of the storm evolution could be erroneously altered (e.g., an initial supercell could evolve into a multicell system if the cold pool propagated too quickly away from the cell).

The domain was 160 km by 200 km in the horizontal and 16 km in the vertical. A mean storm system motion was subtracted from the wind field to keep the simulated convective system within the domain. The horizontal grid spacing was 1 km; the vertical spacing varied smoothly from 260 m at the bottom to 730 m at the top. The horizontal resolution was twice as fine and the ver-

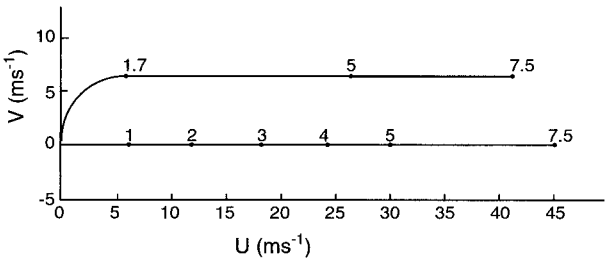

FIG. 6. Idealized hodographs used in the simulation experiments. Heights shown are in km AGL.

tical resolution at low levels also twice as fine as that in the Rotunno et al. (1988) and Weisman et al. (1988) simulations.

The homogeneous environment was characterized by an idealized sounding (Fig. 5) and idealized hodograph (Fig. 6). The basis for our sounding is the one used by Weisman and Klemp (1982), which has a CAPE of 2200 J kg^{-1}, but which we have modified to include a strong cap at the top of the boundary layer and to be relatively dry above the cap (Fig. 5), as is more characteristic of severe weather soundings in the plains (e.g., Bluestein et al. 1988; Bluestein et al. 1989). We were motivated to use the modified sounding, which also has a CAPE of 2200 J kg^{-1}, not only because it is more realistic, but also because we felt that it would be more difficult to trigger secondary convection along outflow boundaries, owing to the increase in convective inhibition. Tests were also conducted with the Weisman–Klemp sounding for comparison with previous studies; little differences were found with previous sounding results.

The idealized hodograph (Fig. 6) exhibits a ''quarter-circle'' clockwise turn up to 1.7 km above the ground, and linear vertical shear above, up to 7.5 km AGL, with a constant vertical shear magnitude of 6×10^{-3} s^{-1}. Above 7.5 km, the wind is kept at a constant magnitude of 42 m s^{-1}. This hodograph is clearly characteristic of the supercell regime (Weisman and Klemp 1982, 1984, 1986). Simulations were also completed for unidirectionally sheared (straight) hodographs, with some of the more significant differences discussed below, as well as for hodographs confined to only the lowest 5 km AGL, with only minor differences noted from the primary results reported here (not discussed further).

For the simulations of line segments of cells, we varied the orientation of the hodographs in each of the following ways (Fig. 4): we oriented the section of the hodographs above the region of curvature (i.e., above 1.7 km) normal, at a 45° angle, at 135°, and parallel to the line of thermal bubbles. These hodograph orientations correspond to various commonly found situations in nature (Beebe 1956; David 1976). Let α denote the angle the shear vector above 1.7 km rotated in a clockwise manner from the line of forcing. We now briefly note what α is for some typical synoptic patterns. The $\alpha = 0°$ case corresponds to a north–south-oriented line of forcing in southerly flow in middle and/or upper levels in the troposphere (e.g., if there is a negatively tilted trough at 500 mb to the west of the line of forcing), a

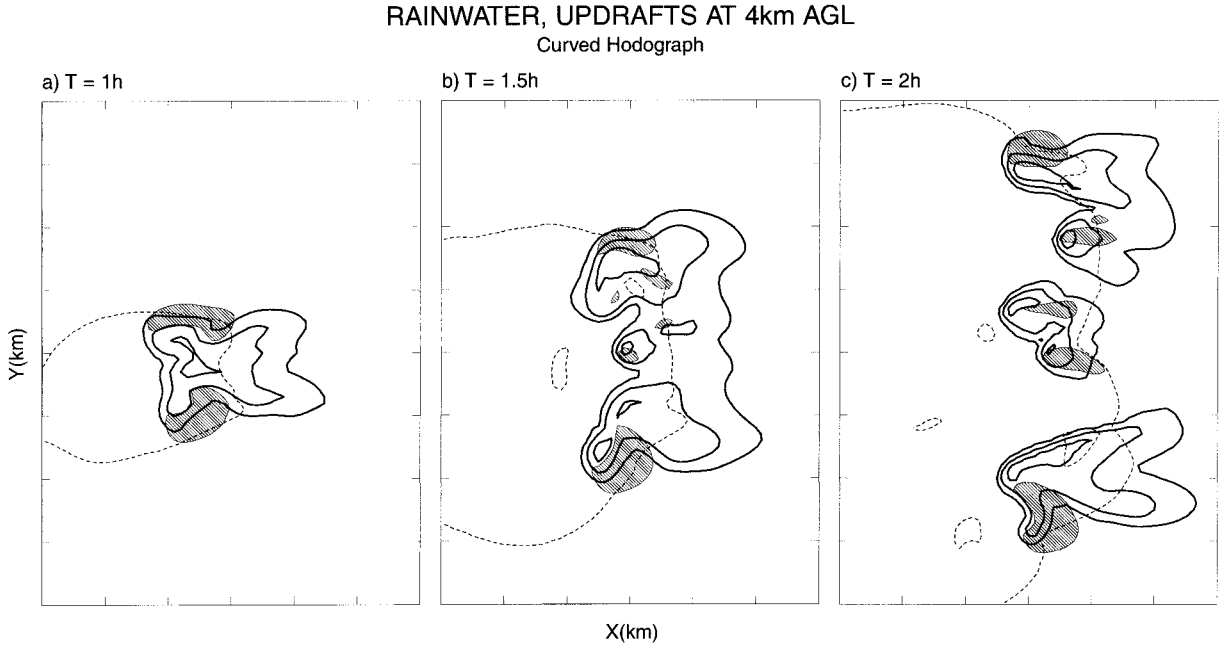

FIG. 7. Simulated fields for an isolated thermal bubble, at 1, 1.5, and 2 h, of liquid-water mixing ratio (thick contours at 1, 4, and 8 g kg^{-1}) and vertical velocity (shaded region in excess of 8 m s^{-1}) at 4 km for the modified sounding and curved hodograph. Tick marks are spaced 10 km apart. Gust front at 0.25 km depicted by dashed line (perturbation temperature at 0.25 km, with respect to ambient environment, of -1°C). Only a 60 km $\times$ 80 km portion of the full domain is shown.

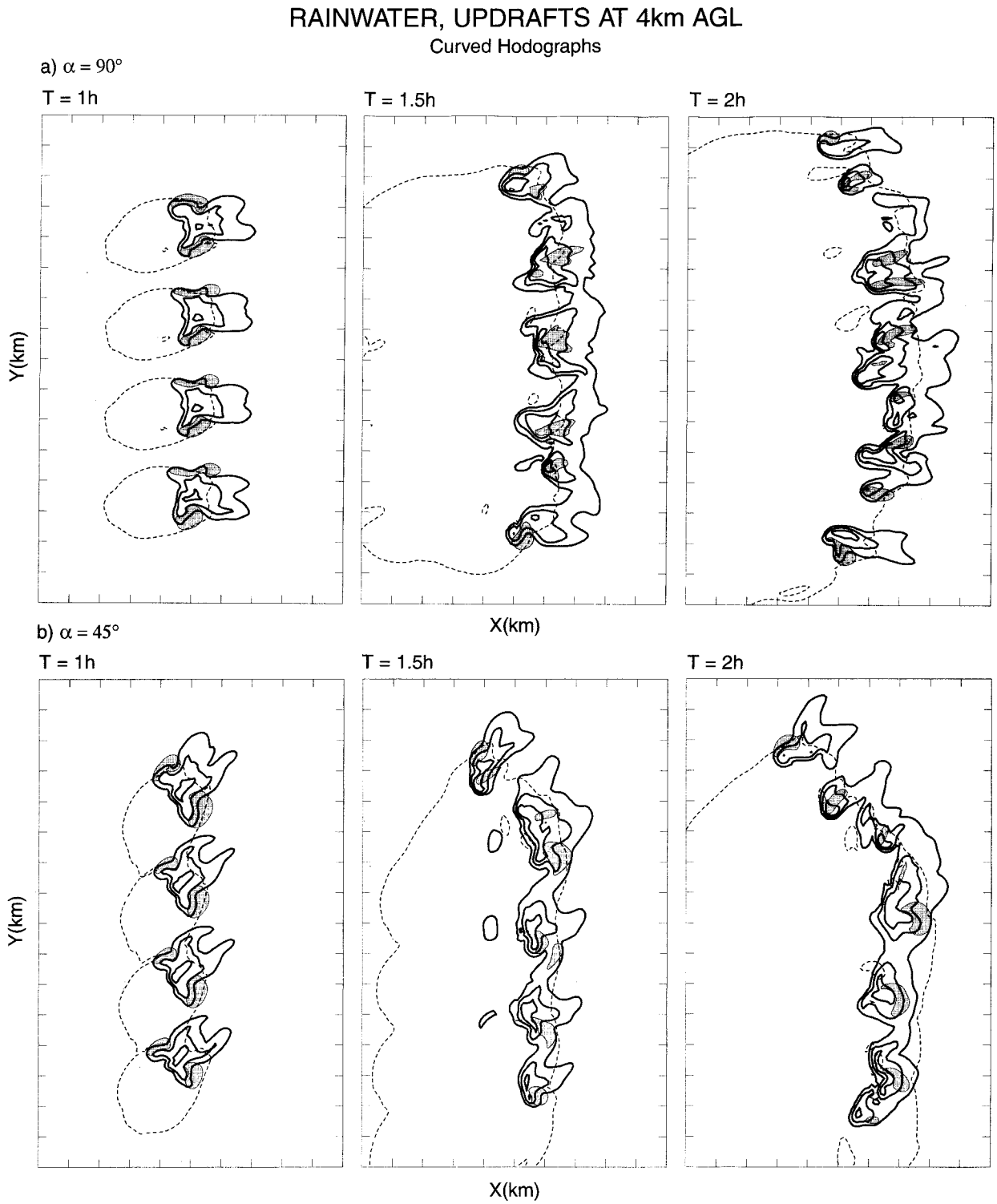

FIG. 8. As in Fig. 7 except for the line simulations when (a) $\alpha = 90°$, (b) 45°, (c) 0°, and (d) 135°. Only a 120 km × 170 km portion of the full domain is shown.

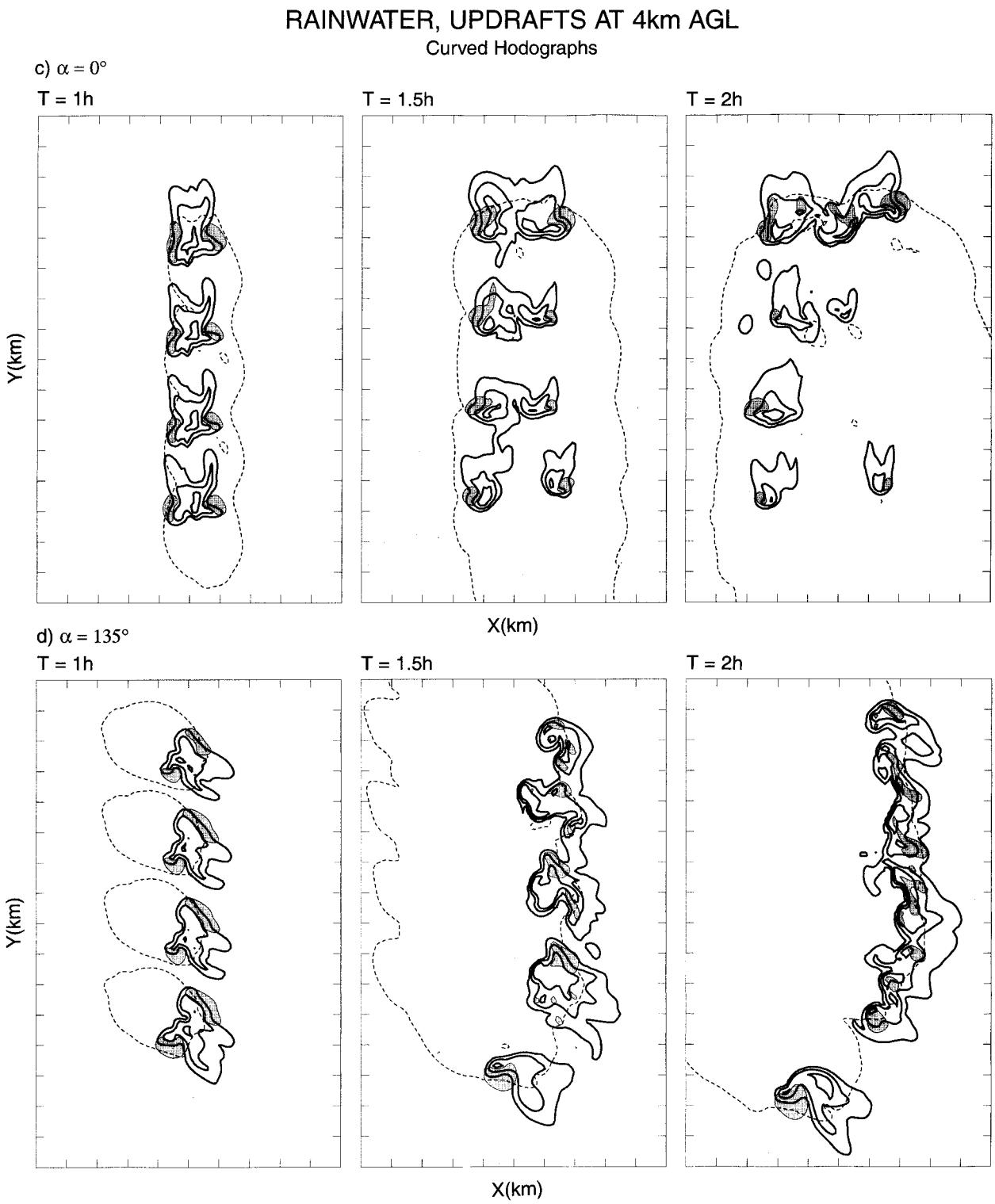

FIG. 8. (*Continued*)

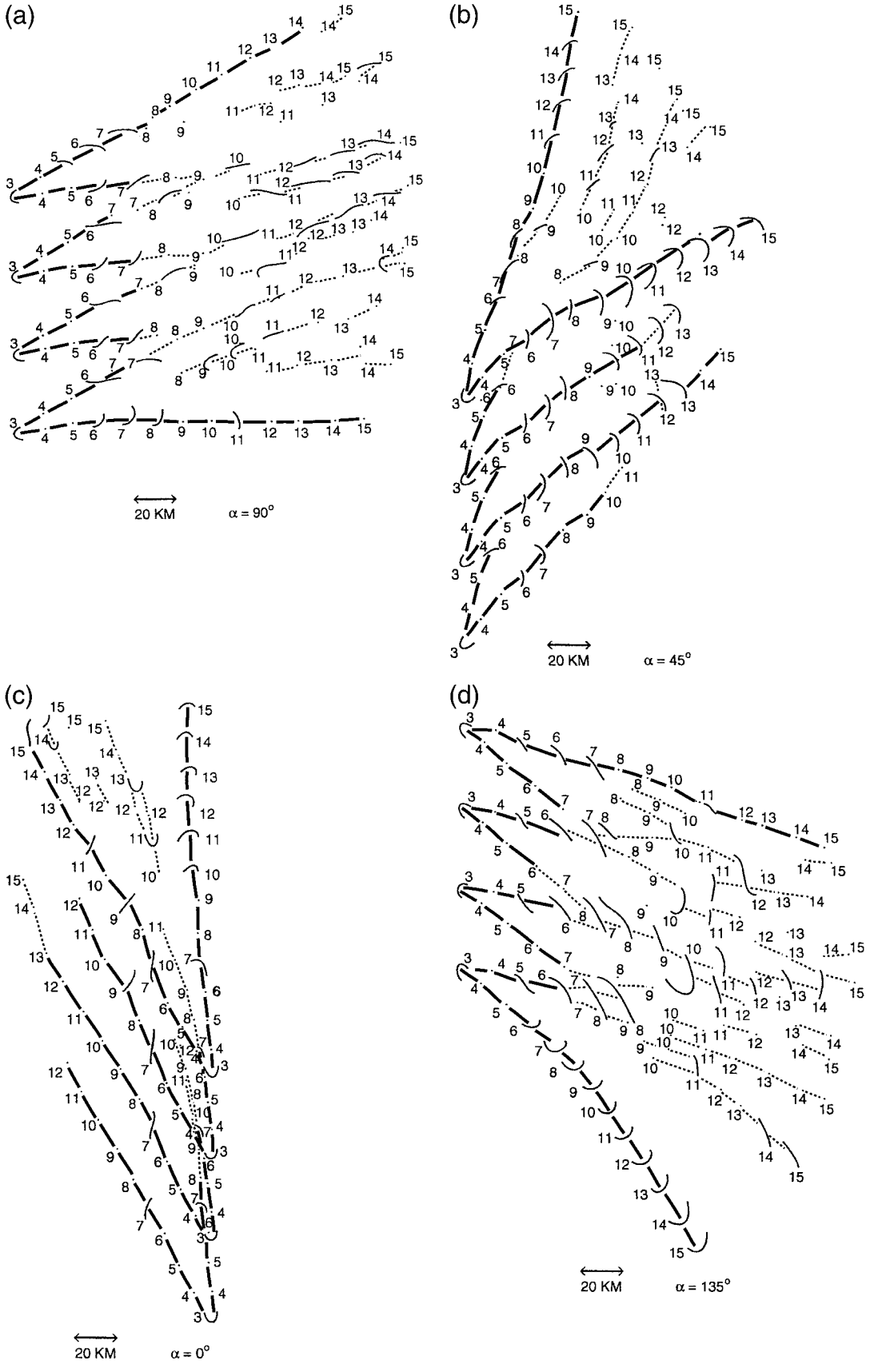

northeast–southwest-oriented line of forcing in southwesterly flow (e.g., if there is a trough at 500 mb to the west), and an east–west-oriented line of forcing in westerly flow (e.g., if there is zonal flow at 500 mb with small amplitude disturbances propagating through). The $\alpha = 45°$ case corresponds to a north–south-oriented line of forcing in southwesterly flow, a northeast–southwest-oriented line of forcing in westerly flow, and an east–west line of forcing in northwesterly flow [e.g., if there is ridge at 500 mb upstream and a trough downstream (Johns 1984)]. The $\alpha = 90°$ case corresponds to a north–south-oriented line of forcing in westerly flow and a northeast–southwest-oriented line of forcing in northwesterly flow. The $\alpha = 135°$ case corresponds to a north–south-oriented line of forcing in northwesterly flow. Other combinations of line-of-forcing and hodograph orientations are possible, but for brevity we have noted only those representative of the most commonly observed combinations.

Finally, we also triggered storms along a line, 15 km west of which there is a warmer, drier air mass (Fig. 4): the water vapor mixing ratio at all levels was decreased to 20% of its normal value; in addition, the temperature below 600 mb was increased west of the interface between the two air masses, so that the hydrostatic pressure gradient force at all levels across the boundary due to any density difference is negligible. The temperature difference across the boundary is 5 K at the ground and decreases with height until it vanishes at 600 mb. These conditions represent, qualitatively at least, a very strong dryline (e.g., Ziegler and Hane 1993; Hane et al. 1993). It is not, however, our intent to simulate dryline dynamics and dryline evolution; rather, we wish to simulate the effects of storm suppression as cells cross a boundary behind which CAPE is decreased substantially or even vanishes. Thus, the dry air behind the boundary is meant also to have a similar effect as the cooler, stable air on the cold side of a front or an outflow boundary. In our case, the CAPE west of the boundary is reduced considerably. The 15-km separation of the thermal bubbles from the drier air mass was chosen so that storms could mature before interacting with the boundary. If the separation were too small, dry air would be advected to the growing storm and prevent it from developing; if the separation were too large, then it would take too long for the effects of the boundary to be felt.

3. Results of simulations

a. Influence of the relative hodograph orientation on system organization, cell type, and movement

For comparison with the line simulations to follow, Fig. 7 presents the evolution of an isolated cell for the thermodynamic and vertical wind shear environments described above. A cell is defined as a convective updraft characterized by a closed region of vertical velocity in excess of 10 m s^{-1} at 4 km AGL. By 1 h, the initial cell has begun to split; updrafts are evident on both the southern and northern flanks of the original rain cell. Rainwater notches are collocated with each of these updraft regions. By 1.5 h, the cyclonic, right-moving cell appears stronger than the anticyclonic left-moving cell, as would be expected with the clockwise curvature of the low-level hodograph. New ordinary cells have also begun to develop along the gust front extending between the two splitting cells. By 2 h, the right-moving cell has taken on the classic signature of a supercell storm, with a well-formed hook, and forward flank notch. The left mover, however, has also maintained significant strength, while more new ordinary cells are developing between the right and left movers.

The cell patterns and structures between 1 and 2 h for the line simulations with different orientations of the vertical wind shear vector may be compared by inspecting Fig. 8. The ground-relative tracks of each of these cells, characterizing their propagation characteristics, longevity, and degree of interactions with neighboring cells, are presented in Fig. 9. In some instances it was easy to locate cells; in others, cells were more difficult to locate precisely because the updraft contours were elliptically shaped. To determine which cells are ordinary cells and which are supercells, we analyzed the evolution and motion of major updraft, precipitation, and vorticity maxima. Supercells are defined as those for which the major updraft rotates cyclonically (anticyclonically), lasts much longer than the time it takes an air parcel to pass up through the updraft from the boundary layer and leave the storm at its top (about 20–50 min), and moves to the right (to the left) of the mean shear. Ordinary cells are short lived, either do not rotate or rotate only weakly, and do not move significantly to the right or left of the mean shear. The cells that we determined to be supercellular are indicated by the thick, solid cell tracks in Fig. 9, while those that were not supercellular are indicated by the thinner, dotted cell tracks.

Overall, the results of the line simulations are qualitatively similar to the conceptualizations presented in the introduction for splitting supercells in unidirection-

←

FIG. 9. Tracks of updraft maxima at 4 km AGL from 0.5 to 2.5 h in ground-relative coordinates. For the modified sounding with a curved low-level hodograph. Only updrafts whose speeds are at least 10 m s^{-1} are tracked. Locations of updrafts are indicated every 10 min; numbers plotted $\times 600$ are the times in s since initiation. Updrafts whose shape is subjectively determined to be elliptical are plotted as line segments along the 10 m s^{-1} major axis. The orientation of the hodograph above 1.7 km with respect to the line of forcing is (a) 90°, (b) 45°, (c) 0°, and (d) 135°. Scale is as indicated. Thick cell tracks signify storms that display significant supercellular characteristics; dotted cell tracks signify ordinary cells.

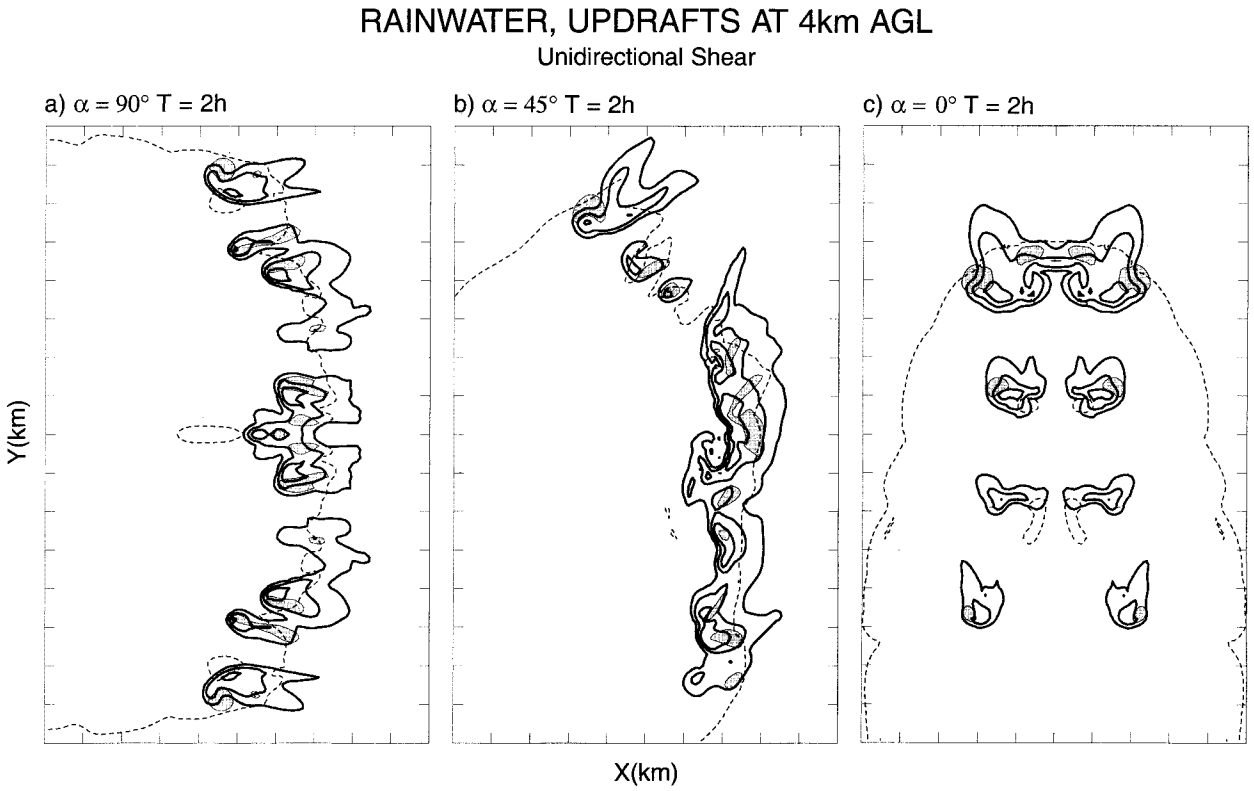

FIG. 10. As in Fig. 8 but for unidirectional shear, with (a) $\alpha = 90°$, (b) 45°, and (c) 0°, only at 2 h.

ally sheared environments. The major difference is that the inclusion of the low-level curvature in the hodograph favors the cyclonic, right-moving cells of the splitting pair. However, the finiteness of the line of cells does lead to some unanticipated results, since the degree to which the line-end cells interact with the remaining system varies considerably from case to case. Also, when and where new cells are generated along the spreading cold pools between the original cells differs significantly with the addition of low-level hodograph curvature, as will be described later in this section.

In the case of $\alpha = 90°$ (Fig. 9a), the four initial cells evolve into a number or splitting cells during the first hour, oriented along the line of forcing, along and just behind the surface cold pool (Fig. 8a). The cyclonic, right-moving updraft is stronger than the anticyclonic left-moving updraft owing to the bias imposed by the low-level clockwise curvature to the hodograph (Rotunno and Klemp 1982; Weisman and Klemp 1984). The evolution of each individual storm in the line is quite similar during this time period, as neighboring cells do not interact with each other until 1.3–1.5 h. Only the anticyclonic left-moving cell at the northern end of the line and the cyclonic right-moving cell at the southern end of the line are able to evolve relatively independently from the other cells. These end supercells appear nearly as if only a single cell were initiated along the line of forcing (e.g., Fig. 7). The splitting cells between the end cells begin to interact after an hour, producing a much more complicated array of apparent cell types and properties. After about 1.5 h, a new series of ordinary cells forms along the leading edge of the cold pool, which complicates the evolution along the line even further. Overall, after 2 h, the only cells that have retained classic supercell characteristics are the end left- and right-moving cells resulting from the original cell splits at the ends.

The reader is referred to Fig. 1, Fig. 8a, and Fig. 9a for a cursory comparison between the idealized numerical simulations and a real case. In Fig. 1, for which $\alpha = 90°$, the southernmost cell and its neighbor to its north interact as the the left mover from storm 2 collides with the right mover from storm 3; the right mover from storm 2 becomes isolated and develops pronounced supercell characteristics (Bluestein and Woodall 1990).

The early evolution for the case of $\alpha = 45°$ (Fig. 9b) is quite similar to that of the $\alpha = 90°$ case, in that the initial cells split into left- and preferred right-moving supercells. However, by 1 h, the left-moving cells have now moved into the cold, stable, surface outflow of the neighboring right-moving cells, and quickly dissipate between 1 and 1.5 h. The only exception is the northernmost anticyclonic left mover, which maintains its identity throughout the entire 2.5-h simulation. Without the left movers to interact with, the four initial cyclonic right movers along the line are able to maintain their

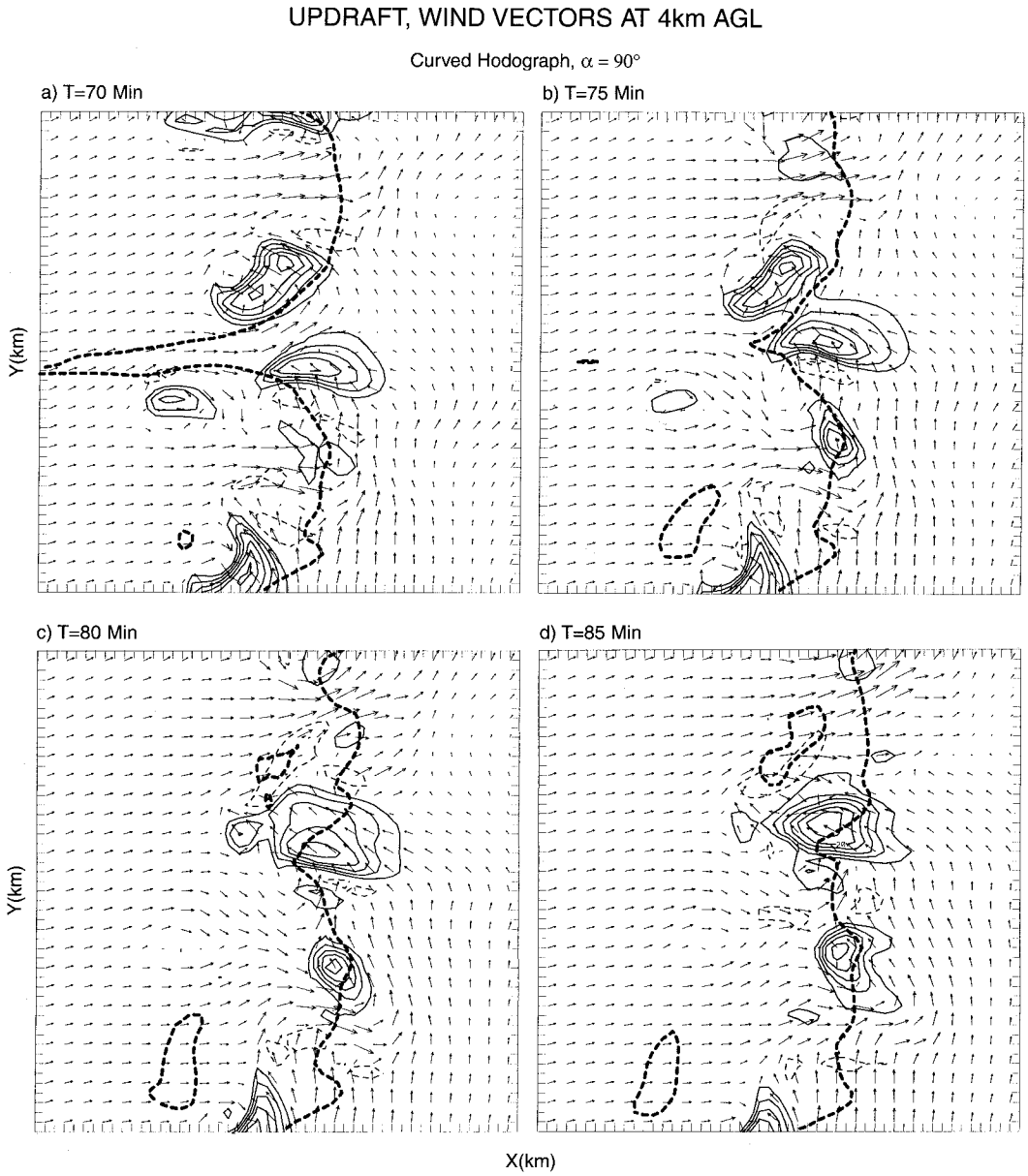

FIG. 11. Simulated system-relative wind field at 4 km AGL depicted by vectors (spacing between each pair of tick marks = 1 km; 1 km = 10 m s^{-1}), at 5-min intervals. Gust front at 0.25 km depicted by dashed line (perturbation temperature at 0.25 km, with respect to ambient environment, of −1°C). Upward vertical velocity at 4 km depicted by solid lines at 4 m s^{-1} intervals; outer contour is at 4 m s^{-1}. Only a 50 km × 50 km portion of the full domain is shown. For the modified sounding with a curved hodograph and $\alpha = 90°$.

identity to 2 h and beyond in some cases, before new cell development and interactions with the neighboring outflows create a more complicated pattern. Contrary to our expectations, the southernmost right mover in this case weakens by 2 h, because it encounters the outflow from the storm to its north and becomes located well within the surface cold air; thus, the CAPE is reduced. This cell also does not propagate to the right as much as the other right movers after 90 min [because its updraft weakens (not shown)], further enhancing the interaction with its neighbor to the north (Fig. 8b).

When $\alpha = 0°$ (Fig. 9c), the initial storms again split; however, in this case the anticyclonic left movers survive longer than the cyclonic right movers because the left movers are better able to keep up with the westward-expanding cold pool, owing to the low-level hodograph curvature. This behavior will be discussed in the next section. The strongest cells remaining after 2 h are along the downshear (northern) side of the surface cold pool, including the original right and left movers from the initial splitting of the northernmost cell in the line, along with some newly developed ordinary cells in between.

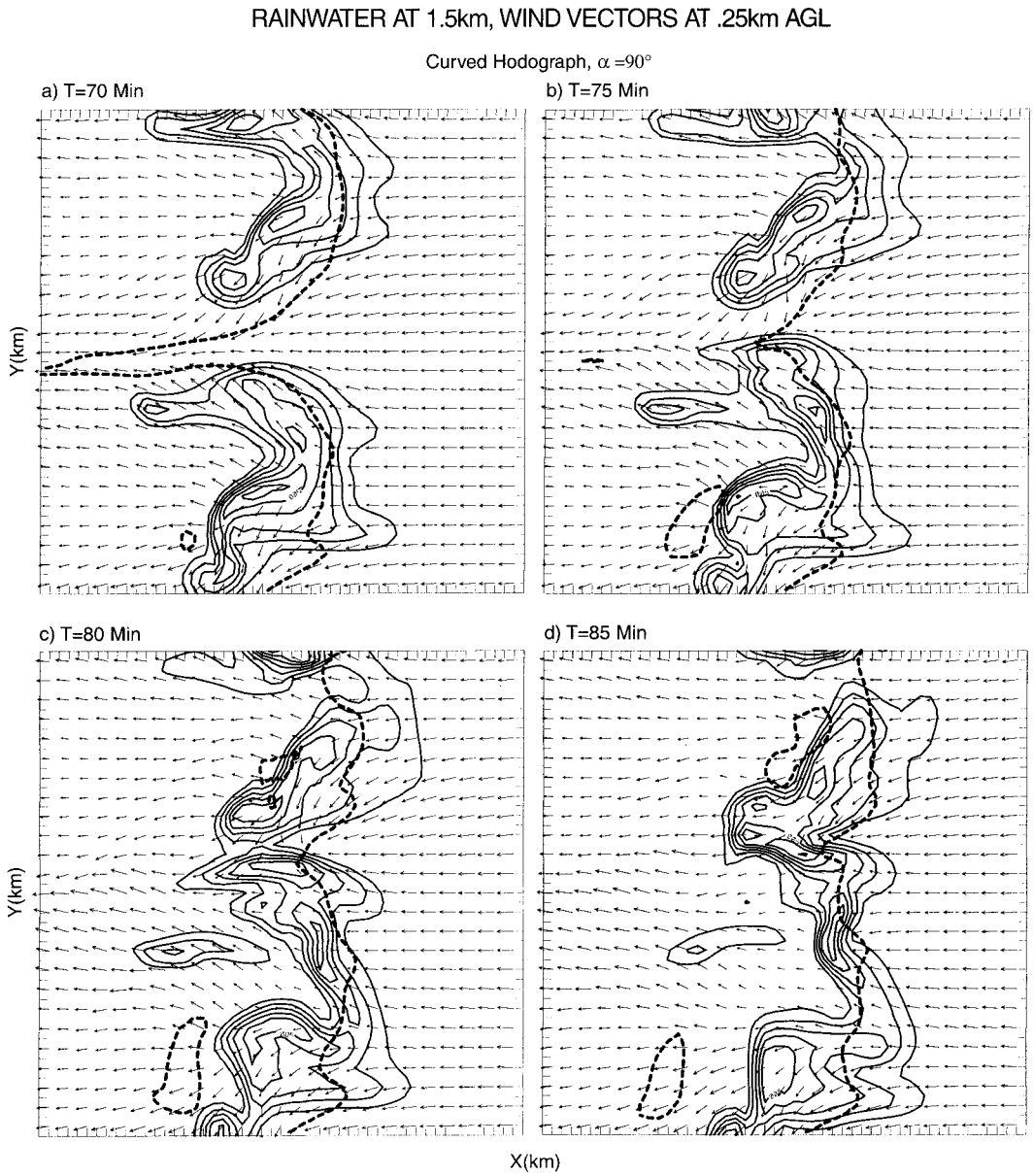

FIG. 12. Simulated system-relative wind field at 0.25 km AGL depicted by vectors (spacing between each pair of tick marks = 1 km; 1 km = 10 m s^{-1}), at 5-min intervals. Liquid-water mixing ratio (g kg^{-1}) at 1.5 km AGL is depicted by solid lines at 1 g kg^{-1} intervals; outer contour represents 1 g kg^{-1}. Gust front depicted as in Fig. 11. Window is same as in Fig. 11. For the modified sounding with a curved hodograph and $\alpha = 90°$.

Finally, for $\alpha = 135°$ (Fig. 9d), the early evolution of the system is somewhat similar to that for the case in which $\alpha = 45°$, but rotated about the axis normal to the line of forcing, since, except below 1.7 km, the two shear profiles are symmetric about the axis normal to the line of forcing. Neighboring left- and right-moving cells interact after 1 h, except at the ends of the line. However, after this time the system evolves into a multicellular squall line between the end cells. The southernmost cyclonic supercell is the strongest produced in any of the presented cases, appearing much as in the isolated cell simulation (Fig. 7), with a quintessential hook and forward flank notch apparent by 1.5 h. This cell becomes increasingly separated from the rest of the convective system, remaining well defined past 2.5 h.

b. Effects of hodograph curvature

The addition of low-level clockwise curvature to a hodograph can have two primary effects. First, the right-moving supercell tends to be more intense than the left-moving supercell (Klemp and Wilhelmson 1978; Weis-

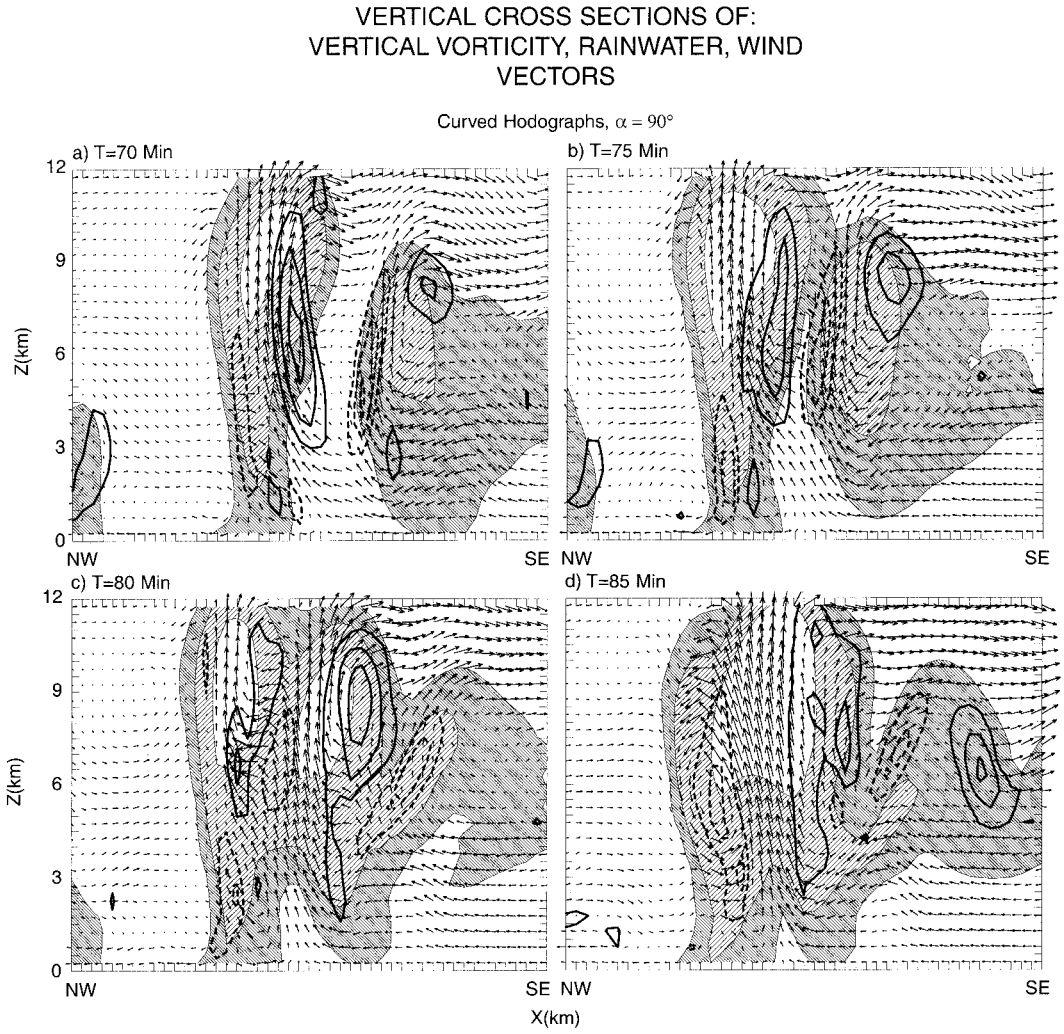

FIG. 13. Vertical cross section oriented at 150° (NW–SE) through the southernmost left mover and the nearest right-moving neighbor to the north shown in Figs. 11 and 12, of wind (a vector length of one grid interval represents 12 m s^{-1}), vertical vorticity (contoured at a 50×10^{-4} s^{-1} interval, with the zero contour omitted), and rainwater (darkly stippled between 1 and 4 g kg^{-1}, lightly stippled between 4 and 10 g kg^{-1}, and clear above 10 g kg^{-1}) at (a) 70, (b) 75, (c) 80, and (d) 85 min.

man and Klemp 1984), if each has equal access to the identical warm, moist, ambient surface air mass. In addition, according to Rotunno–Klemp–Weisman (RKW) theory (Rotunno et al. 1988), the best condition for new cell growth along the leading edge of a cold pool occurs where the low-level ambient horizontal vorticity vector is oriented in the opposite direction to the low-level vorticity generated at the edge of the cold pool (i.e., in the downshear direction). Thus, adding low-level curvature to the hodograph can change the region along the spreading ouflow where new cells are most apt to be generated.

The impact of hodograph curvature in the above experiments is summarized in Fig. 10, which presents the overall storm structure at 2 h for the unidirectional shear simulations for the $\alpha = 90°$, 45°, and 0° cases, as described in Figs. 8a–c. The $\alpha = 135°$ unidirectional shear case (not shown) is a mirror image of the $\alpha = 45°$ unidirectional shear case; anticyclonic, left-moving cells are maintained within the interior of the line rather than cyclonic, right-moving cells.

For the $\alpha = 90°$ case (cf. Fig. 8a at 2 h and Fig. 10a), the overall impact or system evolution is small; the most noticeable difference by 2 h is that in the curved hodograph case the cyclonic, right-moving cell at the southern end of the system is enhanced compared to the anticyclonic, left-moving cell at the northern end of the system.

For the $\alpha = 45°$ simulations (cf. Fig. 8b at 2 h and Fig. 10b), the most prominent difference is the tendency for the right-moving supercells within the line to remain more isolated in the curved hodograph case. The more multicellular character of the line for the unidirectional shear can be directly related to the RKW effect. In particular, the low-level horizontal vorticity has a signifi-

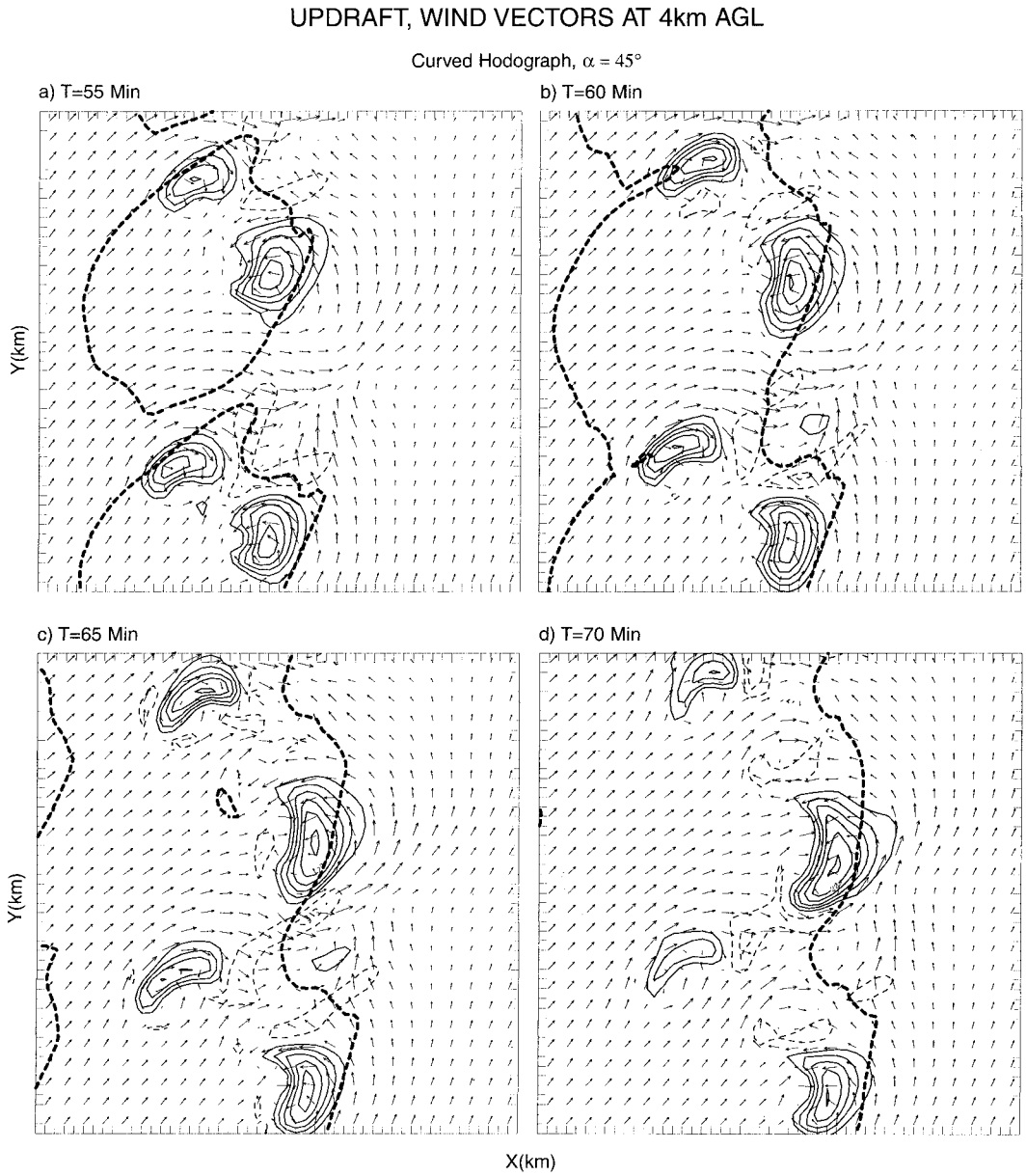

FIG. 14. Same as Fig. 11 but for $\alpha = 45°$.

cant component in the direction opposite to that of the cold-pool-generated vorticity generated at the eastern edge of the system in the unidirectional case. However, in the curved shear case, the low-level vorticity has a significant component in the same direction as the cold-pool-generated vorticity. Thus, we would expect stronger, deeper lifting and more new cell growth along the edge of the cold pool in the unidirectional shear case. Also, the anticyclonic left-moving cell at the northern end of the line is strongest in the unidirectional-shear case, as would be expected, since clockwise hodograph curvature tends to weaken the anticyclonic, left-moving members of a split pair. The favoring of the northernmost left-moving supercell over the southernmost right-moving supercell for both the straight- and curved-shear cases (because the latter supercell moves into the cold outflow of its neighbor) emphasizes that cell geometry can be just as important as hodograph curvature in favoring right- or left-moving storms.

Finally, the RKW effect has a significant impact on the overall evolution of the $\alpha = 0°$ case as well (cf. Fig. 8c at 2 h and Fig. 10c). For unidirectional-shear, the low-level horizontal vorticity vector is directed normal to the horizontal vorticity that is generated solenoidally along the left and right sides of the spreading cold pool. The strongest cell growth would thus be expected along the northern edge of the spreading cold pool (Fig. 10c) where the solenoidally generated vor-

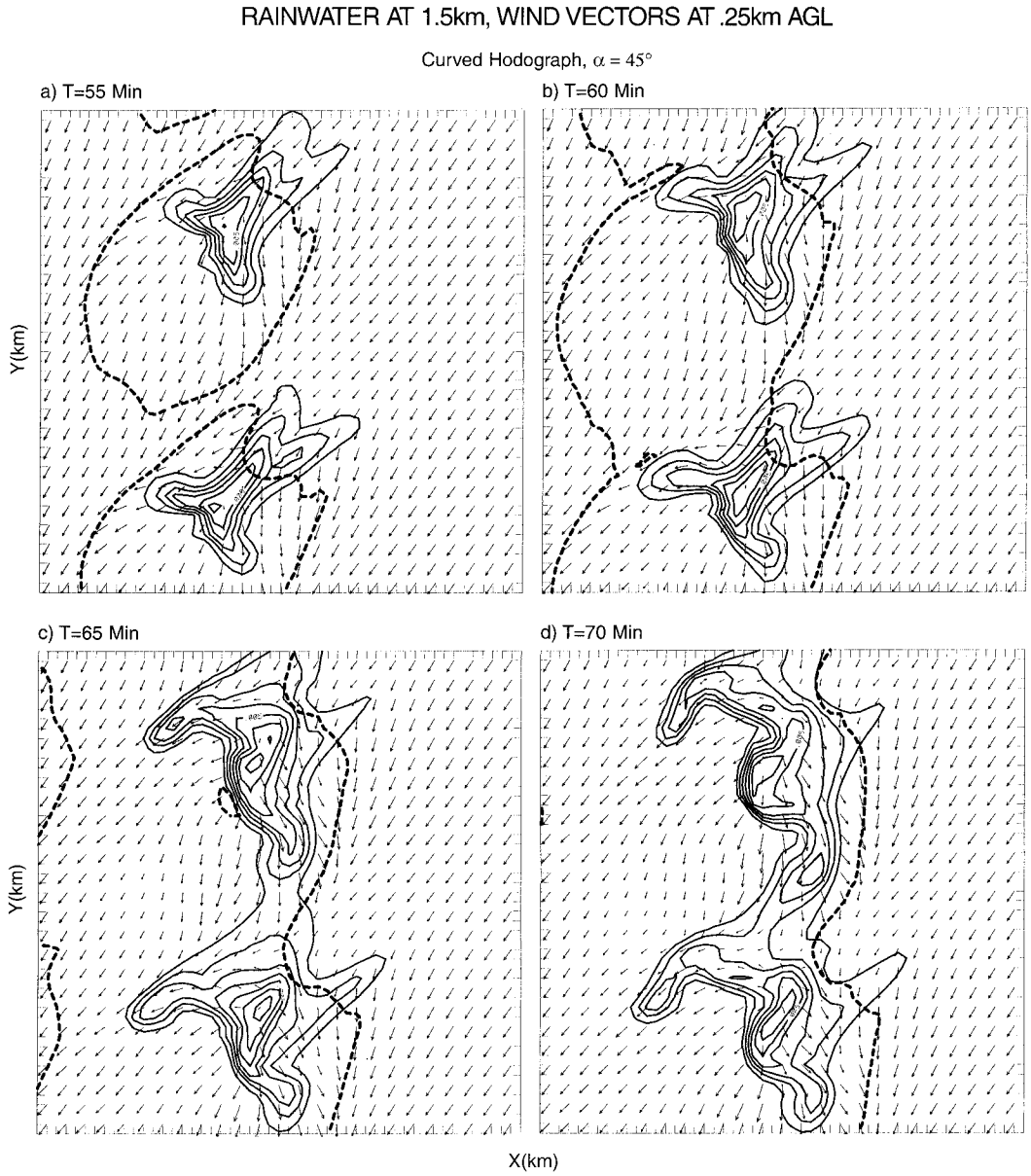

FIG. 15. Same as Fig. 12 but for $\alpha = 45°$.

ticity is opposite in sign to the horizontal vorticity associated with the vertical shear. On the other hand, in the curved-hodograph case, the low-level horizontal vorticity vector is directed opposite in direction to the low-level vorticity that is generated solenoidally along the western edge of the surface cold pool. Thus, cell growth and longevity would be expected to be enhanced also on the western portion of the system, as is evident in Fig. 8c. More subtle effects due to low-level hodograph curvature are also evident for the $\alpha = 45°$, 90°, and 135° cases, which affect the manner in which the individual cells interact within the lines, as will be discussed in the next section.

c. Storm interactions

It is seen in Figs. 8 and 9 how some cells either do not interact with neighboring cells or continue to evolve as if neighboring cells have no discernible effect, while others do interact with their neighbors and subsequently either behave differently than isolated cells do or decay. There are two basic types of interaction that we have identified. 1) Updrafts collide with neighboring updrafts. 2) Updrafts collide with neighboring surface cold pools, but do not interact with neighboring updrafts. To illustrate the nature of neighboring cell interactions, we will focus on the interaction of the left-moving member

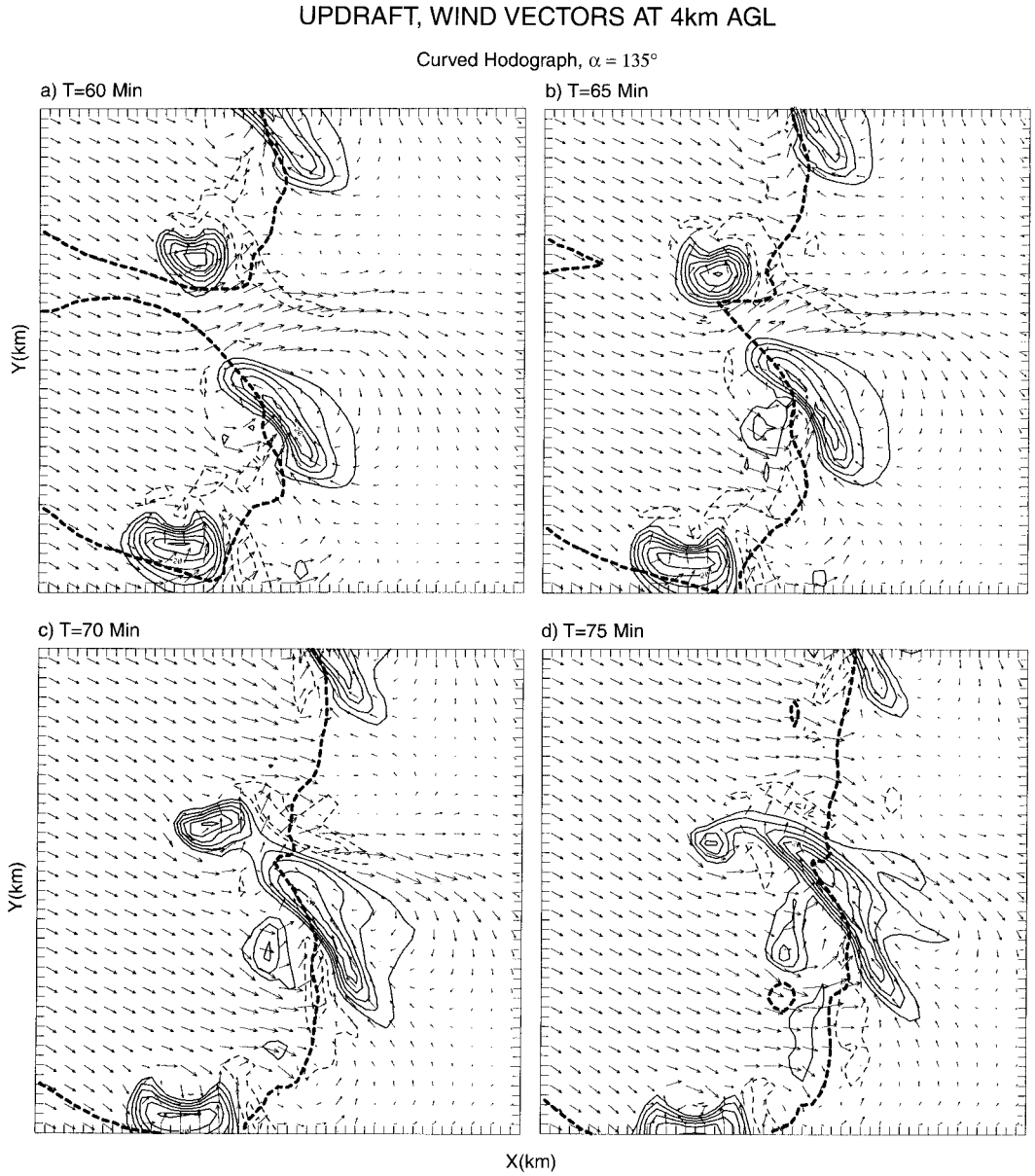

FIG. 16. Same as Fig. 11 but for $\alpha = 135°$.

of the split cell at the southern end of the line with its right-moving neighbor to its north.

We consider the $\alpha = 90°$ case first (Figs. 11 and 12). At 70 min, the updrafts at 4 km AGL have yet to display any significant interactions, as the surface gust fronts have yet to collide (Fig. 11a). The right-moving updraft to the north and left-moving updraft to the south are within 13 km of each other. A significant portion of the left-moving updraft leads the gust front. It is not clear why it leads the gust front as much as it does. Future studies are needed to understand why updrafts can lead gust fronts, rather than remain along their leading edges. This behavior, however, is again consistent with RKW theory, since the low-level ambient horizontal vorticity vector points toward the west, opposite to the vorticity generated behind the northward-progressing cold pool. However, the right-moving updraft remains more tilted behind the gust front, as the low-level ambient horizontal vorticity points in the same direction as the cold-pool-generated vorticity along this southward-moving gust front. At 75 min (Fig. 11b), the surface gust fronts have completely merged, while the left-moving cell intensifies in the notch region just ahead of the colliding gust fronts. The right-moving cell, however, has begun to weaken. At 80 min (Fig. 11c), the left-moving cell has remained strong, while the right-moving cell has continued to weaken. Finally, by 85 min (Fig. 11d), the colliding right- and left-moving cells have been replaced

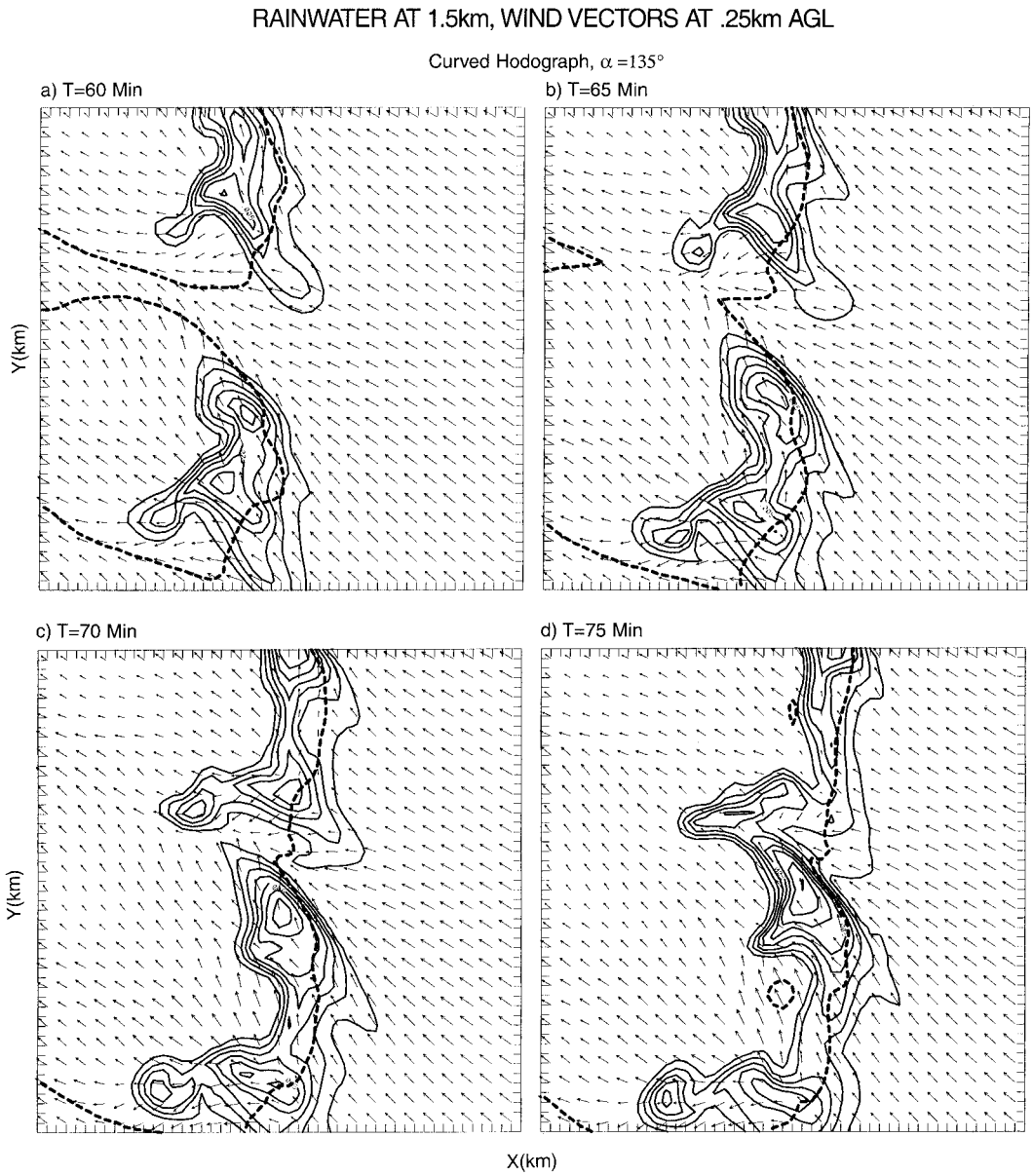

FIG. 17. Same as Fig. 12 but for $\alpha = 135°$.

by a single, strong cell. The rainwater field at 1.5 km AGL (Fig. 12) further reflects the evolution evident in the midlevel updraft field; the northern right mover is quite strong at 70 min (there is a hook in the rainwater field), but subsequently weakens as the left mover approaches, and a new rain core develops in the notch region between the colliding surface gust fronts from 75 to 85 min. This new cell maintains its identity for a relatively long time (e.g., Fig. 9a).

It is also interesting to consider what happens to the midlevel rotation as the storms interact (Fig. 11). At 70 min, the northern, right-moving updraft clearly displays cyclonic rotation, while the left-moving updraft displays anticyclonic rotation. However, as the cells approach and collide, the rotational attributes become less clearly defined; the new updraft that develops in the notch region ahead of the gust fronts displays no significant rotational correlation at all. Instead, the updraft region is characterized by a vortex couplet, one of the hallmarks of a new cell developing in a sheared environment. However, this new cell does not evolve into a supercell, but rather remains an ordinary cell, since the updraft remains well behind the leading edge of the cold pool (not shown).

The interactions between the two cells can be clarified further through the analysis of vertical cross sections through the cores of the two updrafts during this same time period (Fig. 13). At 70 min, the updrafts and rain-

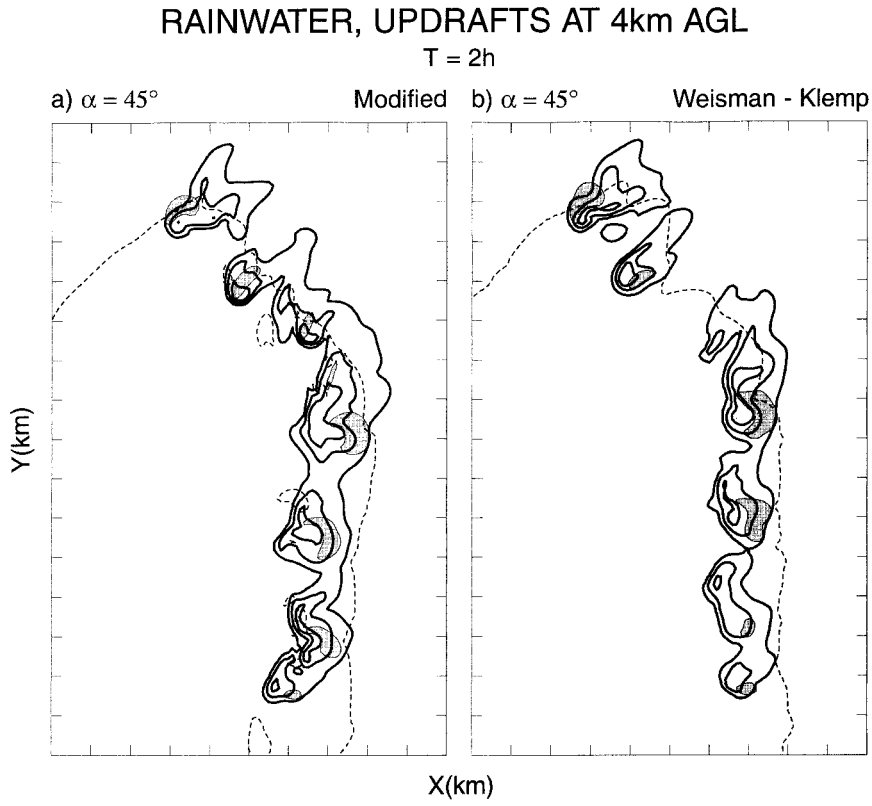

FIG. 18. Effects of varying moisture and stability. Panel to left represents simulation at 2 h for modified sounding; right panel is for unmodified sounding. Otherwise as in Fig. 8b.

water fields are still completely separate, and there is no significant vertical circulation in between the cells. (Note that the vertical cross section cuts through the core updraft of the southern cell but does not go through the core of the rainwater field, which is southwest of the updraft region.) The northern updraft is quite a bit stronger than the southern updraft at this time; the northern rainwater field displays a classic overhang, as is often characteristic of supercell storms. The vertical cross sections also clearly depict the predominantly cyclonic character of the northern updraft and anticyclonic character of the southern updraft. As the cells move closer to each other, a new updraft begins to develop between the cells at low levels (Figs. 13b,c), and by 85 min (Fig. 13d) a single, very strong updraft has taken the place of the two original updrafts. As this is occurring, the rainwater fields merge aloft, even though a relatively distinct new updraft has grown from below. The vertical vorticity–updraft correlations evident earlier also weaken, and the updraft at 85 min is characterized by a vortex couplet (cyclonic to the south, anticyclonic to the north) as also noted above.

So, in this case, neither the updrafts nor the liquid-water maxima actually merge. Instead, a new updraft and associated liquid-water maximum form when the two earlier cells get within 10 km or so of each other and the gust fronts have collided in between the two updrafts aloft.

A similar analysis for the $\alpha = 45°$ case (Figs. 14 and 15) indicates that, unlike in the $\alpha = 90°$ case, the mid-level updrafts from the right- and left-moving updrafts are not on a direct collision course, but are affected primarily through the collisions of the surface gust fronts. This collision has the biggest impact on the left-moving cell, which intensifies briefly as it intercepts the gust front from the northern cell, but then quickly dissipates as it becomes surrounded by cold, stable surface air (Fig. 14). The low-level rainwater field shows a similar chronology (Fig. 15); both the two original right-moving supercells survive. The northern right mover appears a bit larger and stronger than the southern storm at 70 min. Both supercells have evolved from a classic to more of a high-precipitation character (Moller et al. 1994) during this time period, as the updrafts and notches in the rainwater field have shifted from the southwestern flank of each cell to the eastern (forward) flank of each cell.

Finally, in the $\alpha = 135°$ case (Figs. 16 and 17), the cyclonic northern right mover now collides with the gust front from the southern anticyclonic left mover, intensifying briefly before decaying. The left mover is able to maintain its identity throughout this interaction, in-

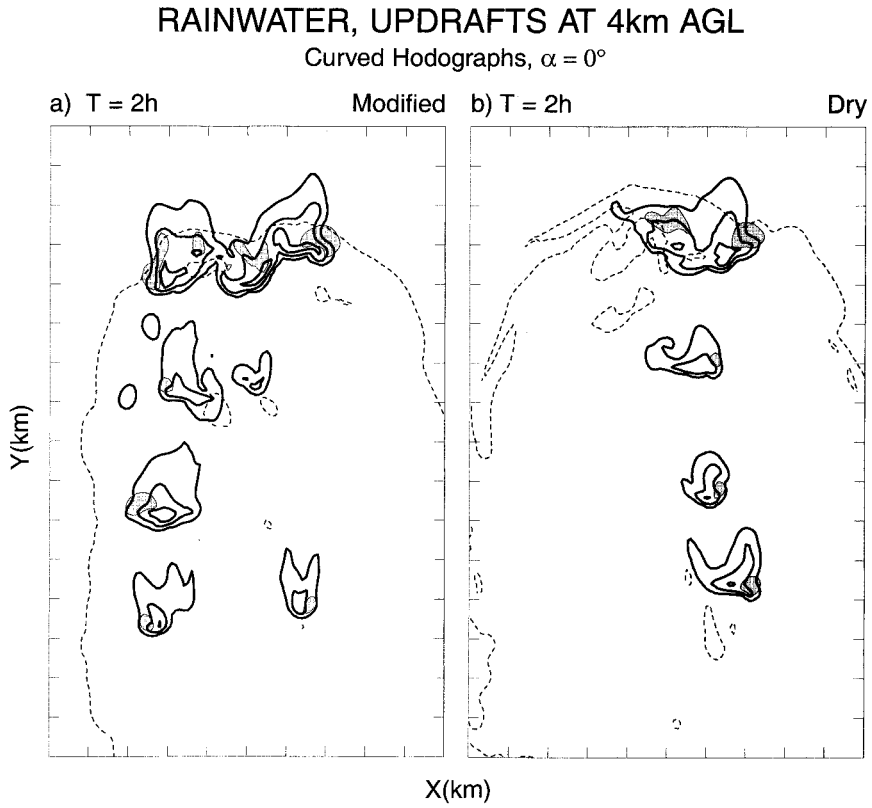

FIG. 19. Effects of dry air to the west of the boundary. (left) Simulation at 2 h for modified sounding; (right) case of dry air to the west of the boundary. Otherwise as in Fig. 8c.

cluding maintaining anticyclonic updraft rotation at midlevels. The low-level rainwater field of the left mover also intensifies somewhat after the interaction with the northern cell's gust front (Fig. 17). As noted earlier, the cyclonic, right-moving cell at the southern end of this system displays the most classic supercell structure of any of the cases presented, probably because it interacts the least with other cells (Fig. 9d), just like in the isolated cell simulation presented in Fig. 7.

d. Sensitivities to midlevel moisture, capping inversions, and dry air to the west of the boundary

An entire set of simulations as described above were also completed using the Weisman and Klemp (1982, 1984, 1986) sounding, which exhibits a much weaker capping inversion as well as much more moisture at midlevels than for the present cases. Since there have been many simulation results presented in the literature using the Weisman–Klemp sounding, we felt it would be instructive to compare its use for the present study as well.

There were few qualitative differences between simulations using the original Weisman–Klemp sounding and those using the present sounding (e.g., Fig. 18). In a few cases (i.e., in those with curved low-level hodographs and $\alpha = 45°$), small cells behind the cold pool found in the Weisman–Klemp sounding simulations were suppressed or absent in the present simulations.

Since the boundaries along which convective storms form in nature often separate dry boundary layer air from moist boundary layer air (i.e., along the dryline and some fronts), it is possible that some cells may cross the boundary to its dry side, or that the dry air aloft crosses the boundary and catches up to some of the convective cells triggered along it. Simulations were therefore done to determine the effect of the dry air.

The overall effect of dry air to the west of the boundary, for the $\alpha = 0°$ case, was to weaken the left-moving members of the splitting supercells as they crossed the boundary (Fig. 19). For the other cases (not shown), the boundary's evolution affects storm behavior and we therefore will not consider it.

4. Summary and discussion

The numerical simulation experiments show that supercells within lines are most likely to develop in a high-shear, moderate-CAPE environment when the motion of cells is such that they do not interact with any of their neighbors; they behave as they do in experiments in which storms are triggered by isolated thermal bubbles. Other intense, long-lived, rotating cells having supercell characteristics can form, but they are modified by col-

lisions with neighbors and or interactions with cold-pool boundaries.

1) When the deep-layer shear is normal to the line of forcing, isolated, cyclonically (anticyclonically) rotating, right-moving (left-moving) supercells develop at the end of the line to the right (left) of the deep-layer shear. A squall line having embedded, but distinct, intense cells develops in between. The squall line develops after neighboring right- and left-moving cells collide. The cells in the squall line have some supercellular characteristics, but the updrafts at midlevels are not very well correlated with vertical vorticity.
2) When the overall shear is 45° (135°) from the line of forcing, a line of cyclonic (anticyclonic) supercells can be maintained for long periods of time (e.g., more than 2 h). In addition, when $\alpha = 45°$ (135°), an isolated, anticyclonically (cyclonically) rotating, left-moving (right-moving) supercell is prominent at the downshear end of the line. (It is noteworthy that, owing to neighboring storm interactions, a prominent anticyclonically rotating supercell persists when $\alpha = 45°$, even when the low-level curvature in the hodograph favors right-moving supercells.) When $\alpha = 135°$ and the low-level hodograph favors cyclonically rotating supercells, the other cells along the line become multicellular.
3) When the overall shear is parallel to the line of forcing, an isolated, cyclonically rotating, right-moving supercell forms on the downshear side of the line of forcing. A left-moving storm also persists on the downshear end of the line but is more multicellular in character.

These results confirm that the ends of lines of forcing are preferred locations of isolated supercell development. However, which end or whether both ends support supercells depends upon the relative orientation of the vertical shear with respect to the line. The end cells have only one neighbor with which they can interact or compete, and motion that is significantly deviant from that of their inner neighbors allows them to behave like isolated cells. Cells with cyclonic supercell characteristics are most likely to exist in the interior of the line when $\alpha = 45°$.

It was found that storm behavior for an environment characterized by the Weisman–Klemp sounding differed quantitatively, but not qualitatively, than that for an environment characterized by different static stability and drier air aloft.

Since the formation pattern of convective storms can be monitored by Doppler radar and/or satellite imagery, and environmental hodographs can be determined from nearby soundings or wind profilers, if they are available, or from gridpoint data from numerical models, it should be possible to see if our numerical results can be applied to the nowcasting or short-term forecasting of convective storms. We also plan to examine many past cases to see if observational data can be used to confirm the numerical results.

Storm interactions as viewed by Doppler radar may not give a complete picture of the nature of the interactions. For example, our numerical results suggest that a new updraft can be induced just before two updrafts/reflectivity maxima actually collide. The subsequent new reflectivity maximum lags and is not coincident with the new updraft maximum. Or, it may appear as if reflectivity maxima converge, while in nature a completely new updraft may be forming.

The results from our simulations also suggest that more experiments be conducted to determine further which variables control the nature of neighboring cell interactions. In this study we have detailed only a few specific types of interactions. Controlled experiments should be undertaken in which the sensitivity of cell interactions to variations in the shear profile, the CAPE, the timing of the initial cell triggering, and cell spacing could be determined. Are there some interactions that are not destructive? Although cell collisions in our experiments usually resulted in cells that were not as intense as those that were isolated, we did find one instance in which the collision of cells led to an increase in low-level vorticity for a short period of time (not shown). Perhaps in nature this process might be associated with the brief formation of a tornado. However, the enhancement of surface vorticity may be highly dependent on the timing of the interactions. Currently, interactions occur relatively early in the life cycle of each storm, before the surface vorticity features have had a chance to mature (it usually takes 90–120 min). Future studies will have to consider the impact of such timing issues.

Another issue that needs to be explored is the theoretical basis for the observed spacing between cells and the timing of cell formation. What parameters in nature determine the spacing and timing? Is there an optimum spacing and timing for the formation of supercells? We suggest that efforts be undertaken to find answers to these questions.

Acknowledgments. This study was funded by NSF Grants ATM-9302379 and ATM-9612674. The first author is grateful to the Mesoscale and Microscale Meteorology (MMM) Division of the National Center for Atmospheric Research (NCAR) for providing facilities to work on this study during his sabbatical leave in 1996 and during the summers of 1997 and 1998. Computer time was provided by the Scientific Computing Division at NCAR. The authors are also indebted to Jody Williams, Pat Waukau, and Bill Boyd for their assistance with the MMM computing system, and to David Dowell and Tom Condo for their help with computing facilities at OU. Rich Rotunno, Joe Klemp, Bill Skamarock, and Matt Gilmore provided insightful comments.

REFERENCES

Beebe, R. G., 1956: Tornado composite charts. *Mon. Wea. Rev.,* **84,** 127–142.

Bluestein, H. B., and M. H. Jain, 1985: Formation of mesoscale lines of precipitation: Severe squall lines in Oklahoma during the spring. *J. Atmos. Sci.,* **42,** 1711–1732.

——, and G. R. Woodall, 1990: Doppler-radar analysis of a low-precipitation (LP) severe storm. *Mon. Wea. Rev.,* **118,** 1640–1664.

——, and S. Parker, 1993: Modes of isolated, severe convective-storm formation along the dryline. *Mon. Wea. Rev.,* **121,** 1354–1372.

——, and T. Hutchinson, 1996: Convective-storm initiation and organization near the intersection of a cold front and the dryline. Preprints, *Seventh Conf. on Mesoscale Processes,* Reading, United Kingdom, Amer. Meteor. Soc., 538–540.

——, and D. R. MacGorman, 1998: Evolution of cloud-to-ground lightning characteristics in the Spearman, Texas, tornadic supercells of 31 May 1990. *Mon. Wea. Rev.,* **126,** 1451–1467.

——, E. W. McCaul Jr., G. P. Byrd, and G. Woodall, 1988: Mobile sounding observations of a tornadic storm near the dryline: The Canadian, Texas storm of 7 May 1986. *Mon. Wea. Rev.,* **116,** 1790–1804.

——, ——, ——, ——, G. Martin, S. Keighton, and L. C. Showell, 1989: Mobile sounding observations of a thunderstorm near the dryline: The Gruver, Texas storm complex of 25 May 1987. *Mon. Wea. Rev.,* **117,** 244–250.

Burgess, D. W., and E. B. Curran, 1985: The relationship of storm type to environment in Oklahoma on 26 April 1984. Preprints, *14th Conf. on Severe Local Storms,* Indianapolis, IN, Amer. Meteor. Soc., 208–211.

David, C. L., 1976: A study of upper air parameters at the time of tornadoes. *Mon. Wea. Rev.,* **104,** 546–551.

Hane, C. E., C. L. Ziegler, and H. B. Bluestein, 1993: Investigation of the dryline and convective storms initiated along the dryline: Field experiments during COPS-91. *Bull. Amer. Meteor. Soc.,* **74,** 2133–2145.

Johns, R. H., 1984: A synoptic climatology of northwest flow severe weather outbreaks. Part II: Meteorological parameters and synoptic patterns. *Mon. Wea. Rev.,* **112,** 449–464.

Klemp, J. B., and R. B. Wilhelmson, 1978: The simulation of three-dimensional convective storm dynamics. *J. Atmos. Sci.,* **35,** 1070–1096.

Lilly, D. K., 1979: The dynamical structure and evolution of thunderstorms and squall lines. *Annu. Rev. Earth Planet. Sci.,* **7,** 117–161.

Marwitz, J. D., 1972a: The structure and motion of severe hailstorms. Part I: Supercell storms. *J. Appl. Meteor.,* **11,** 166–179.

——, J. D., 1972b: The structure and motion of severe hailstorms. Part II: Multi-cell storms. *J. Appl. Meteor.,* **11,** 180–188.

——, 1972c: The structure and motion of severe hailstorms. Part III: Severely sheared storms. *J. Appl. Meteor.,* **11,** 189–201.

Moller, A. R., C. A. Doswell III, M. P. Foster, and G. R. Woodall, 1994: The operational recognition of supercell thunderstorm environments and storm structures. *Wea. Forecasting,* **9,** 327–347.

Rotunno, R., and J. B. Klemp, 1982: The influence of the shear-induced pressure gradient on thunderstorm motion. *Mon. Wea. Rev.,* **110,** 136–151.

——, ——, and M. L. Weisman, 1988: A theory for strong, long-lived squall lines. *J. Atmos. Sci.,* **45,** 463–485.

Weisman, M. L., and J. B. Klemp, 1982: The dependence of numerically simulated convective storms on wind shear and buoyancy. *Mon. Wea. Rev.,* **110,** 504–520.

——, and ——, 1984: The structure and classification of numerically simulated convective storms in directionally varying wind shears. *Mon. Wea. Rev.,* **112,** 2479–2498.

——, and ——, 1986: Characteristics of isolated convective storms. *Mesoscale Meteorology and Forecasting,* P. S. Ray, Ed., Amer. Meteor. Soc., 331–358.

——, ——, and R. Rotunno, 1988: Structure and evolution of numerically simulated squall lines. *J. Atmos. Sci.,* **45,** 1990–2013.

Wilhelmson, R. B., and J. B. Klemp, 1983: Numerical simulation of severe storms within lines. Preprints, *13th Conf. on Severe Local Storms,* Tulsa, OK, Amer. Meteor. Soc., 231–234.

Ziegler, C. L., and C. E. Hane, 1993: An observational study of the dryline. *Mon. Wea. Rev.,* **121,** 1134–1151.